Yield of Neutrons per Interaction in U, Pb, W, and Sn by Protons of Six Energies between 250 and 900 Mev Selected from Cosmic Radiation

M. Bercovitch, H. Carmichael, G. C. Hanna, and E. P. Hincks*

Physics Division, Atomic Energy of Canada Limited, Chalk River, Canada

(Received February 15, 1960)

The production of low-energy neutrons in U, Pb, W, and Sn by protons of six selected energies between 250 and 900 Mev has been measured using cosmic radiation as a proton source. The protons were selected and their energy measured by a vertical counter telescope containing three Čerenkov detectors which employed liquid nitrogen, water, and Plexiglas as radiating media. The protons interacted in 22 and 44 g cm^{-2} thick slabs of the target elements, and the neutrons produced were detected in a 4-foot cubic paraffin moderator, $B^{10}F_3$ counter assembly placed below the proton selecting telescope. The principal body of data was obtained at 3260 m altitude; a series of runs at 150 m was made to check the high-altitude data for muon contamination of the selected protons.

The proton-gated neutron rates for the various targets were converted to mean neutron multiplicities per interaction using (a) the efficiency of the neutron detector as measured using calibrated Pu^{240} spontaneous fission and Ra-α-Be neutron sources (b) the interaction cross sections of Chen, Leavitt, and Shapiro. The mean multiplicities per interaction range from 5.8±1.0 for 300-Mev protons on 33 g cm^{-2} thick Sn, to 26.7±4.2 for 820-Mev protons on 44 g cm^{-2} thick U. The multiplicities predicted from the Monte Carlo nucleon cascade calculation of Metropolis et al. and the Monte Carlo evaporation calculation of Dostrovsky et al. are in agreement with the measurements when secondary neutron production in the thick targets is taken into account.

1. INTRODUCTION

SINCE its proposal by Serber,[1] the well known nuclear cascade description of high-energy nuclear interactions has become the starting point for virtually all theoretical predictions of the products of nuclear bombardment by high-energy nucleons. Monte Carlo calculations of various degrees of refinement have been carried out, from early work of Goldberger,[2] to the most recent and extensive work of Metropolis et al.[3] which extends the incident energy range to 1.8 Bev, and takes meson production into account. References to the intervening work may be found in the last reference.

The Monte Carlo calculations predict directly:

(a) The features of the fast nucleon cascade, i.e., the numbers of fast nucleons, their energies and angular distributions.

(b) Nuclear transparency.

(c) The excitation energy remaining in the nucleus after the cascade particles have escaped the nucleus.

Metropolis et al. have compared experimental work pertinent to (a) and (b) with their calculations, and in most cases find the agreement satisfactory.

Excitation energies cannot be observed directly but must be inferred from observations of the yield of particles emitted in the process of deexcitation. Much work has been published on observations of stars produced in photographic emulsions exposed to fast particle beams or cosmic rays. In these experiments the separation of events occurring in the various constituents of the emulsion is uncertain at least for the stars of low prong number, and the range of target elements available is in general restricted to those occurring in emulsions. Cosmic-ray experiments are further handicapped by uncertainty of the nature and energies of the incident particles.

Radiochemical studies of nuclides formed in the spallation of target nuclei by fast nucleons form a large part of the existing literature of high-energy interactions. The average numbers of nucleons emitted in the cascade and deexcitation processes may be determined provided one can accurately estimate the yields of the stable and the very short-lived spallation products which are not accessible to radiochemical analysis.

Evaporation theory must in all cases be used to connect the observed particle yields with the nuclear excitations predicted from the nuclear cascade calculations. This step is somewhat simplified in the case of heavy nuclei and excitations up to several hundred Mev, under which circumstances the high Coulomb barrier restricts the emission of the lower energy particles almost entirely to neutrons. The evaporation calculations of Dostrovsky et al.[4] show that the relationship between the average excitation energy and the average number of neutrons emitted is not very sensitive to the exact values of the evaporation-model parameters used. Thus it is possible to use the nuclear excitations given by the Monte Carlo calculations to predict the numbers of low-energy neutrons expected, and the predictions will not depend strongly on the details of the evaporation theory used.

Published experimental data on neutron yields from high-energy interactions are much less extensive than those pertaining to charged particles. Skyrme and Williams[5] have measured neutron yields resulting from the 150-Mev proton bombardment of nuclei of W and

* Present address: The Enrico Fermi Institute for Nuclear Studies, University of Chicago, Chicago 37, Illinois.

[1] R. Serber, Phys. Rev. 72, 1114 (1947).

[2] M. L. Goldberger, Phys. Rev. 74, 1269 (1948).

[3] N. Metropolis, R. Bivins, M. Storm, A. Turkevich, J. M. Miller, and G. Friedlander, Phys. Rev. 110, 185 (1958); Phys. Rev. 110, 204 (1958).

[4] I. Dostrovsky, P. Rabinowitz, and R. Bivins, Phys. Rev. 111, 1659 (1958).

[5] D. M. Skyrme and W. S. C. Williams, Phil. Mag. 42, 1187 (1951); Results quoted by E. E. Gross in reference (6).

Ag. Gross,[6] working at a proton energy of 190 Mev, has measured the yields and energy spectra of neutrons emitted from thin targets of Al, Ni, Ag, Au, and U. Metropolis *et al.* find good agreement between the predictions of their calculation and the results of Gross. Gol'danskii *et al.*[7] have measured the numbers of neutrons produced by 120 Mev and 380-Mev neutrons incident on thick targets of elements ranging from carbon to lead. At higher energies, the only published experiments are those measuring neutron production in various materials by cosmic rays such as those of Montgomery and Tobey,[8] Cocconi,[9] and Ortel.[10] These experiments give no indication of the nature and energies of particles initiating specific events.

We have measured the yields of neutrons resulting from the interaction of cosmic-ray protons in the energy range 250 to 900 Mev with various target nuclei of high atomic weight. We selected individual cosmic-ray protons (which in the selected energy range comprise $\sim 2\%$ of the total cosmic-ray particle flux at 3000 m altitude and $\sim\frac{1}{2}\%$ at sea level), measured their energies to within 100 Mev, and observed the neutrons resulting from their interaction with targets of tin, tungsten, lead, and uranium.

The experiment was carried out in a trailer laboratory at Echo Lake, Colorado, 3260 m above sea level, with a series of control runs at Deep River, Ontario, 150 m altitude. The high altitude observations consisted of a series of preliminary experiments performed in 1954 and early 1955 and a final series with elaborated apparatus performed in early 1956, the results of which are reported here. The Deep River runs occupied a period from July, 1956, to April, 1957. The results of the runs near sea level, where the cosmic-ray muon-proton ratio is larger than that at 3000 m by a factor of about five, were used to check the mountain data for muon contamination of the proton beam.

2. APPARATUS

2.1 The Proton Selector

(a) Description

The proton selector consisted of a vertical cosmic ray telescope formed by two trays of Geiger counters GC_1 and GC_2 (Fig. 1), operated in 4-fold coincidence with two rows of proportional counters, PC_1 and PC_2, and a stack of three Čerenkov detectors $CV_{1,2,3}$ overlapping

[6] E. E. Gross, University of California Radiation Laboratory Report UCRL–3330, 3337, 1956 (unpublished).

[7] V. I. Gol'danskii, A. E. Ignatenko, A. I. Mukhin, V. S. Pen'kina and V. A. Shkoda-Ulyanov, Phys. Rev. **109**, 1762 (1958).

[8] C. G. Montgomery and A. R. Tobey, Phys. Rev. **76**, 1478 (1949).

[9] G. Cocconi, V. Cocconi-Tongiorgi, and M. Widgoff, Phys. Rev. **79**, 768 (1950).

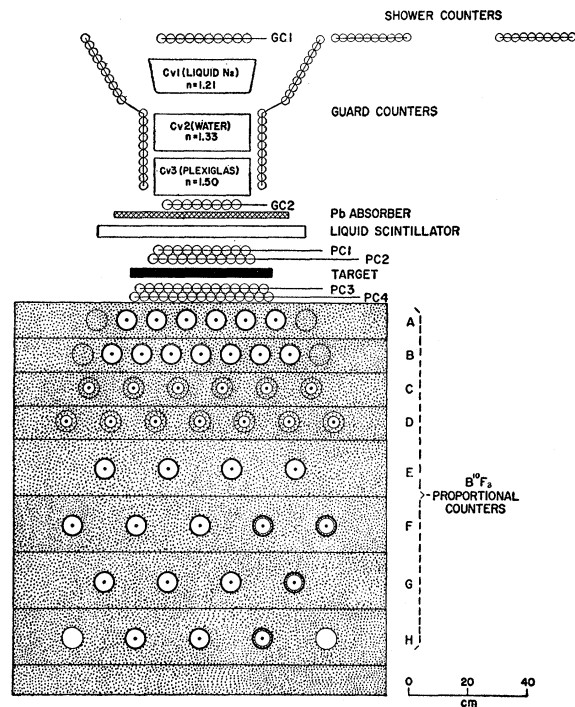[10] W. C. G. Ortel, Phys. Rev. **93**, 561 (1954).

FIG. 1. Experimental arrangement.

the solid angle of the telescope. The radiating media of the Čerenkov detectors were liquid nitrogen, distilled water, and Plexiglas, which have refractive indices of 1.205, 1.33, and 1.50, respectively.

Details of the liquid nitrogen detector are shown in Fig. 2. The nitrogen container was a rectangular, transparent plastic dish, 14 in. by 16 in. by 5 in., made of $\frac{1}{8}$ in. Plexiglas sheet, and set into an evacuated outer shell. The space between the plastic dish and the supporting steel cradle was filled with hard-packed magnesium oxide powder to provide good light reflection. The space between cradle and the outer shell was filled with Santo-Cel insulation, and continuously pumped to a pressure of 5 microns to reduce heat conduction. The Čerenkov light was detected by three end-window EMI-6260 photomultipliers. The tube ends were immersed to a depth of 1 cm into the liquid nitrogen to provide good optical coupling between the liquid and the photocathodes which covered both the ends and the immersed part of the sides. Experience with standard tubes of various types (RCA 5819, EMI 6260, DuMont 6292) had shown very severe deterioration of sensitivity, resolution and stability when immersed in liquid nitrogen. The tubes finally used were specially made by the manufacturer with evaporated iron-substrate photocathodes to improve their conductivity at low temperatures.

The Plexiglas detector consisted of a solid block of plastic, 14 in. by 14 in. by 6 in., surrounded by magnesium oxide powder, placed inside a thin-walled,
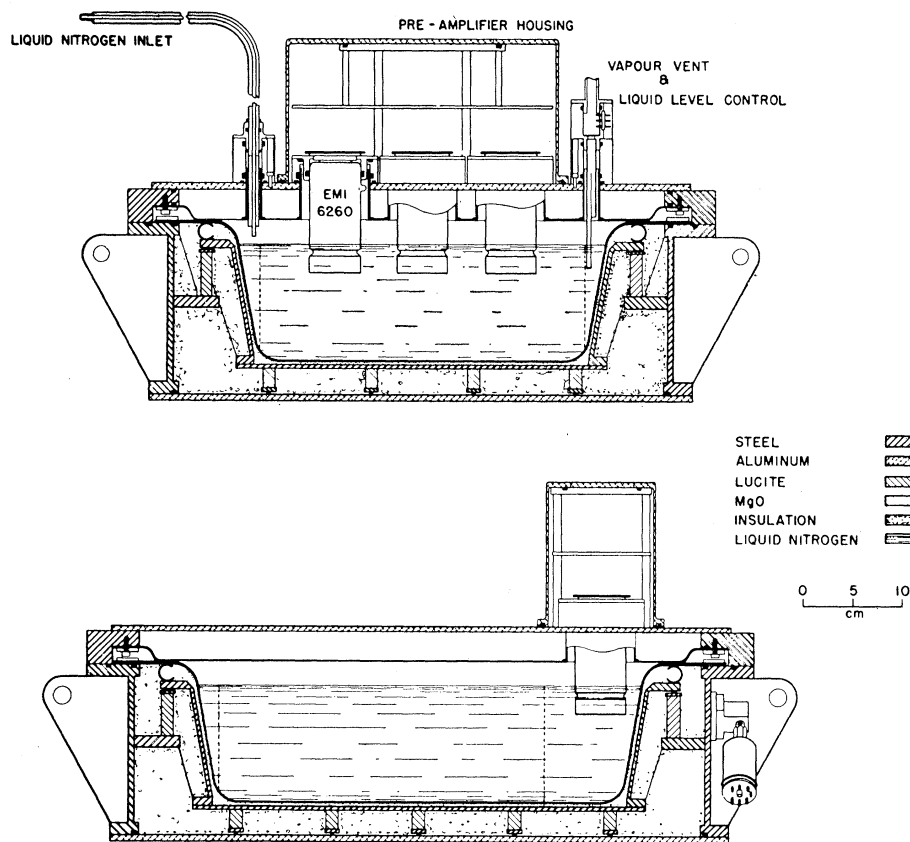
FIG. 2. Liquid nitrogen Čerenkov detector.

STEEL
ALUMINUM
LUCITE
MgO
INSULATION
LIQUID NITROGEN

light-tight aluminum box. Two EMI–6260's, centrally positioned and inset to a depth of 1 cm, on opposite sides of the block were used to detect the light. The water detector, similar in size and shape, consisted of a water-filled box made of $\frac{1}{16}$-in. Plexiglas sheet and surrounded by MgO powder.

A 22 g cm^{-2} thickness of lead absorber was placed below GC$_2$, to increase the total amount of material in the telescope, and to shield the Geiger counters from γ rays emitted by the uranium targets. The remaining γ-ray background in the GC$_2$ tray, 350 counts per second, shortened the life of the counters and made replacement necessary several times during the experiment. Proportional counters rather than Geiger counters had to be used in the two lowermost trays of the telescope, where the background singles rate in the PC$_2$ tray with the 103 kg uranium target in place was $\sim$40 000 counts per second. These counters, made from $1\frac{1}{4}$ in. o.d. brass tubing of 0.020-in. wall thickness, were 22 in. long and had a 0.001-in. central wire. They were filled to a pressure of one atmosphere with a 75% methane+25% argon mixture (to reduce the Landau spread) and were operated at 2300 volts. The amplified pulses had rise and fall times of 0.1 microsecond. With a one microsecond coincidence resolving time the accidental 4-fold rate was negligible. The net effect of the high-gamma counting rates was to introduce a dead-

time loss of 8% in the 4-fold rate, $\frac{3}{4}$ of which was due to the Geiger counter dead-time.

A liquid scintillator[11] $29\frac{1}{4}$ in. square and $1\frac{1}{2}$ in. thick was placed above the PC$_1$ tray to measure the rate of energy loss of selected particles prior to their entry into the target material. Below the target was situated another double tray of proportional counters, PC$_{34}$, in one microsecond coincidence, to detect the emergence of downward-going charged particles from the target.

The telescope was boxed in as completely as possible with Geiger counters to detect particles emerging from or entering the telescope obliquely. Two air shower detecting trays were used on a level with GC$_1$. The top tray of Geiger counters, GC$_1$, was split centrally so that events in which both halves were triggered could be recorded. The lower tray, GC$_2$, was split by connecting alternate counters in parallel in order to detect multiple particles emerging from CV$_3$. These precautions enabled a variety of events which were not protons, but which could trigger the telescope and actuate the Čerenkov detectors so as to look like protons, to be eliminated.

[11] This counter, which has been fully described by C. H. Millar, E. P. Hincks, and G. C. Hanna [Can. J. Phys. **36**, 54 (1958)], was added in the final phase of the experiment, and rendered the proportional counters PC$_1$ and PC$_2$ largely redundant. The latter were retained however, in the interest of reliability.

(b) Principles of Operation

Moving charged particles emit Čerenkov radiation when their velocity exceeds the velocity of light in the surrounding medium. The intensity of the radiation per unit distance in a medium of index of refraction n, is, according to the classical theory of Frank and Tamm,

$$I = e^2/c^2 \int_{\beta n > 1} (1 - 1/\beta^2 n^2) \nu d\nu$$
$$= \text{const.}[1 - 1/\beta^2 n^2] = I_{max}\left(\frac{1 - 1/\beta^2 n^2}{1 - 1/n^2}\right), \quad (1)$$

where $\beta(=v/c)$ and e are the velocity and charge of the moving particle, respectively, ν is the frequency of the emitted light, I_{max} is the asymptotic value of I as $\beta \to 1$, and n has been considered constant over the range of frequencies detected.

This formula has been experimentally verified for mesons passing through Plexiglas for a range of velocities from $\beta_{threshold} = (1/n)$ to $\beta = 0.99970$.[12,13] Figure 3 shows I/I_{max} plotted as a function of $(\gamma - 1)$, the kinetic energy of the particle in units of the rest mass, i.e.,

$$\gamma - 1 = E_{kin}/M_0 c^2 = (1 - \beta^2)^{-\frac{1}{2}} - 1. \quad (2)$$

The pulse-height distribution curve in the nitrogen detector produced by relativistic cosmic-ray muons is shown in Fig. 4. The peak of the distribution occurs at the most probable pulse height for particles with velocity close to c, and was taken to correspond to $I = I_{max}$. The width of the curve which is 65% at half-maximum, is due to the combined effects of photomultiplier statistics and fluctuations in the Čerenkov energy loss. The curves for the Plexiglas and water detectors display better resolution, the width of each distribution being about 50–55% at half-maximum.[13]
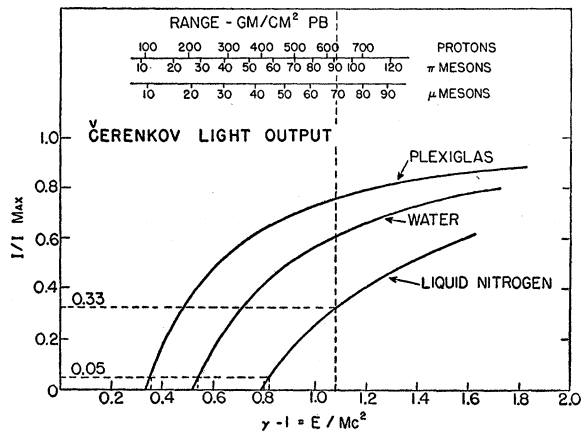
FIG. 3. Calculated relative Čerenkov light intensity as a function of E/Mc^2. The upper scales give the corresponding ranges in Pb of protons, pions, and muons.
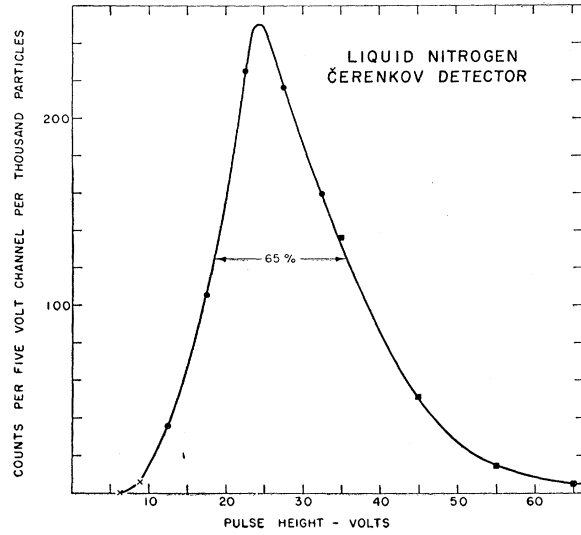
FIG. 4. Pulse-height distribution in the liquid nitrogen Čerenkov detector due to penetrating cosmic-ray particles at sea level.

The proton selector was an elaboration of the "maximum velocity-minimum range" arrangement first described by Duerden and Hyams.[14] In our experiment, heavy particles were selected by requiring that the nitrogen Čerenkov light pulse, if any, in coincidence with a 4-fold telescope coincidence, be smaller than that corresponding to $0.33 I_{max}$. An upper limit was thus set on the velocity of selected particles corresponding to an energy of 1.08 Mc^2 or 1.0 Bev for protons, 150 Mev for pions and 114 Mev for muons. The corresponding ranges in lead are 620 g cm^{-2} for protons, 92 g cm^{-2} for pions, and 70 g cm^{-2} for muons (see Fig. 3). Since the total amount of material in the telescope (including the 22 g cm^{-2} lead absorber) was equivalent in thickness to 145 g cm^{-2} Pb, pions and muons, and less massive particles were in principle excluded,[15] making the apparatus sensitive primarily to protons with incident energies between 0.4 and 1.0 Bev. The corresponding energies of the emergent protons ranged from zero to 0.9 Bev due to ionization loss in traversing the telescope.

Each event combining a 4-fold coincidence and CV$_1$ anticoincidence (the CV$_1$ anticoincidence discriminator, as already stated, being set at a level corresponding to $0.33 I_{max}$) generated a master pulse, which gated, with a resolving time of one microsecond, pulse-height information from the Čerenkov detectors, the proportional counters and the liquid scintillator. The discriminator settings are listed in Table I.

Assuming the initiating particles to be protons, the Čerenkov detectors yielded three independent and overlapping energy measurements, which were required to be consistent within limits set by the resolutions of the individual detectors. Pulse heights from the liquid scin-

[12] J. R. Winckler, E. N. Mitchell, K. A. Anderson, and L. Peterson, Phys. Rev. 98, 1411 (1955).
[13] C. H. Millar and E. P. Hincks, Can. J. Phys. 35, 363 (1957).
[14] T. Duerden and B. D. Hyams, Phil. Mag. 43, 717 (1952).
[15] This amount of material was sufficient to absorb any decay electrons arising from stopped muons.

Table I. Discriminator bias settings for Čerenkov and ionization detectors.

Detector	Disc. no.	Bias	Particle energy
CV_1 (nitrogen)	anticoinc.	$0.33\ I_{max}$	$1.07\ M_0c^2$
	2	0.20	0.94
	1	0.05	0.82
CV_2 (water)	6	1.00	...
	5	0.70	1.30
	4	0.50	0.90
	3	0.35	0.73
	2	0.20	0.63
	1	0.05	0.55
CV_3 (Plexiglas)	7	1.30	...
	6	1.00	...
	5	0.70	0.92
	4	0.35	0.49
	3	0.20	0.41
	2	0.05	0.36
PC_{12}	3	$4.5\times$min. ionization	
	2	$3.0\times$min. ionization	
	1	$1.5\times$min. ionization	
PC_{34}	3	$4.5\times$min. ionization	
	2	$3.0\times$min. ionization	
	1	$1.5\times$min. ionization	
Scintillator	8	$12.0\times$min. ionization	
	7	$6.0\times$min. ionization	
	6	$3.0\times$min. ionization	
	5	$1.6\times$min. ionization	
	4	$1.4\times$min. ionization	
	3	$1.2\times$min. ionization	
	2	$1.0\times$min. ionization	
	1	$0.8\times$min. ionization	

tillator provided an additional check, immediately prior to their passage into the target, on the identity and energy of the particles selected.

After passing through the selector, the protons impinged on the target, which was placed between PC_{12} and PC_{34} centrally with respect to the telescope. The various targets used covered an area 19 in. by 19 in. overlapping the solid angle of the telescope.

2.2 The Neutron Detector

The neutron detector, placed centrally below the proton selector (Fig. 1), was a four-foot cube of paraffin wax in which were placed 42 large $B^{10}F_3$ neutron counters. The counters in Rows A and B were $2\frac{1}{2}$ in. o.d. and had a 22-in. sensitive length. The counter walls were 0.058-in. thick aluminum to minimize the mass of unwanted "target" material in the upper part of the neutron detector, and to decrease the absorption of thermal neutrons in the walls. All other counters had copper walls, the C and D counters having dimensions $1\frac{1}{2}$-in. o.d. by 24 in. sensitive length, and the E, F, G, and H rows $2\frac{1}{2}$-in. o.d. by 36 in. sensitive length. All were filled to a pressure of one atmosphere with 96% enriched $B^{10}F_3$.

The counters were connected singly or in groups to 18 recording channels, which were activated by a 150

microsecond wide gate, delayed 5 microseconds with respect to the master pulse. In this way the lateral and depth distribution in the paraffin of the detected neutrons was obtained. A loss of neutron counts resulted from the inability of the recording system to respond in any given channel to more than one detected neutron per master pulse. An auxiliary circuit, which recorded the combined gated output of all 42 neutron counters, was used to correct for this loss.

3. PERFORMANCE AND CALIBRATION

3.1 Initial Difficulties

It has already been mentioned that a preliminary series of experiments was carried out with less elaborate apparatus. A brief mention of the difficulties that were encountered forms a suitable introduction to a discussion of the performance of the improved apparatus. A fuller account of this early work has been given by Carmichael.[16]

The poor stability of the original liquid nitrogen Čerenkov counter, which was eventually overcome by using special iron-substrate photomultiplier tubes, was responsible for many wasted runs. However, it became clear, as soon as data from both high- and low-altitude stations were available, that more fundamental faults existed in the proton selection apparatus which resulted in a serious contamination of the proton beam by muons. Another symptom of trouble was the occasional occurrence of events in which a very large number of neutrons (one hundred or more) was produced. These were later shown to be associated with showers of cosmic-ray particles.

The muon contamination was attacked in two essentially independent ways. First, boxing in the telescope as far as possible with "guard" trays of Geiger counters reduced the number of events in which a muon entered the telescope from the side accompanied by, for example, a knock-on electron detected in the top counter tray GC_1. Secondly, more stringent tests were applied to the putative proton in the components of the telescope itself. The number of discriminators on both the water and Plexiglas Čerenkov counters was increased from three to six to obtain more detailed information on the light output. This provided a more subtle set of criteria for accepting events as protons than was originally available, when it was possible to eliminate only such comparatively gross anomalies as, for example, the appearance of a detected light signal in both nitrogen and Plexiglas counters with no response from the intervening water counter. Thirdly, a separate useful criterion of acceptability was provided by the liquid scintillator which measured the specific ionization with very much higher resolution than the proportional counters. These tests reduced the probability

---

[16] H. Carmichael, Atomic Energy of Canada Limited Report AECL–UK/C4/112, 1955 and UK/C5/120, 1956 (unpublished).

of an unwanted single particle leaking through the selection apparatus and also tended to eliminate multiple events and thus reinforced the action of the guard counters and of the air shower detecting trays outside telescope on a level with GC_1. Further protection against multiple events was provided by the splitting of GC_1, and by the interleaving of the counters of the GC_2 tray which helped to reject events in which the proton interacted in the telescope.

3.2 The Performance of the Proton Selector

(a) Energy Assignment of Proton Events

Since experimental calibration of the proton selector with protons of known energy was not feasible, it was necessary to calculate its response. From the theoretical Čerenkov intensity-energy variation and the resolution curves of the three Čerenkov detectors experimentally determined using relativistic cosmic-ray muons, we calculated the probability $P_E(a,b,c)$ that a proton emerging from the telescope with energy E is detected as a Čerenkov event (a,b,c), where a, b, and c form a three-digit code indicating the number of discriminator levels tripped by detectors $CV_{3, 2, and 1}$, respectively. In this calculation the ionization loss in traversing the telescope components was taken into account.

Curves were plotted of P_E vs E for all (a,b,c) combinations that were calculated to occur with any appreciable probability. If it is assumed that the incident cosmic-ray proton energy spectrum is flat in the 200–900-Mev region, then the area under each curve gives the relative frequency of occurrence of the corresponding Čerenkov combination to be expected from protons. Certain combinations, particularly many that had probability zero or nearly zero for a proton, occurred with frequencies far in excess of those calculated. These excesses could be attributed to the effects of showers, interactions in the material of the telescope, etc. The remaining observed frequencies were found to be roughly proportional to those calculated.

For the final analysis of the data, only those categories of proton events having the highest calculated probability of occurrence (i.e., those satisfying the most stringent Čerenkov consistency criteria) were retained, since in these cases the smallest proportions of events of nonprotonic origin were expected. These retained events were then subjected to further selection by removing all events accompanied by shower particles passing through GC_1, GC_2, or any of the surrounding guard counters; also events giving scintillator or proportional counter responses inconsistent with those expected for protons of the measured energy were removed.

We summarize in Table II statistics showing the relative effectiveness of the various selection devices at Echo Lake.

As expected, the percentage of rejections by the auxiliary selection devices is much lower for events

TABLE II. Effectiveness of the various selection devices at Echo Lake.

Mean 4-fold rate $= 8220$/hr.
Mean master pulse rate $= 353$/hr.
Fraction of events accepted $= 29\%$ of total Master Pulses ($= 102$/hr.)
Fraction of events rejected $= 71\%$ of total Master Pulses

	% of total master pulse rate	% of the rejected events
Fraction rejected by Čerenkov detectors	63	89
Fraction rejected by scintillator (A events)	22	31
Fraction rejected by PC_{12} (B events)	18	25
Fraction rejected by shower trays, guard trays and split GC_1 (C events)	16	23
Fraction rejected by split GC_2 (D events)	6	9

	Percentage rejected by			
	A	B	C	D	$A,B,C,$ or D
In events *accepted* by Čerenkov detectors	9	13	6	2	22
In events *rejected* by Čerenkov detectors	28	20	22	9	45

falling within the accepted Čerenkov categories than for those outside.

Figure 5 shows the calculated energy distribution within the various selected energy groups with the mean energies and the upper and lower deciles of the distributions marked. These were obtained by lumping together the selected groups covering similar energy bands, and then adding the individual distributions.

(b) Effectiveness of the Selection Criteria

Evidence in support of the energy assignments is given by Fig. 6, which shows the most probable pulse heights observed in the liquid scintillator relative to that of minimum ionizing muons as a function of the mean energy of each proton group. The selection of these groups was as described in 3.2(a), with the exception that no scintillator selection was exercised. The curve is the theoretically calculated one, as described in the paper of Millar et al.[17] and the agreement is considered to be a satisfactory confirmation of the energy assignment of the selected proton groups.

However, even a large muon contamination would have little effect on the most probable pulse height, and the best evidence that this contamination is small is from a comparison of the Echo Lake and Deep River data. The observed ratio of proton rates for the various energy groups is shown in Table III. All energy groups are in satisfactory agreement with the accepted[18] ratio of 10 except the highest, where the disagreement is due to muon leakage in the highest energy channel of the telescope.

[17] C. H. Millar, E. P. Hincks, and G. C. Hanna, Can. J. Phys. **36**, 54 (1958).
[18] A summary of the experimental data is given by G. Puppi and N. Dallaporta, *Progress in Cosmic-Ray Physics*, edited by J. G. Wilson (North Holland Publishing Company, New York, 1952), chap. VI.
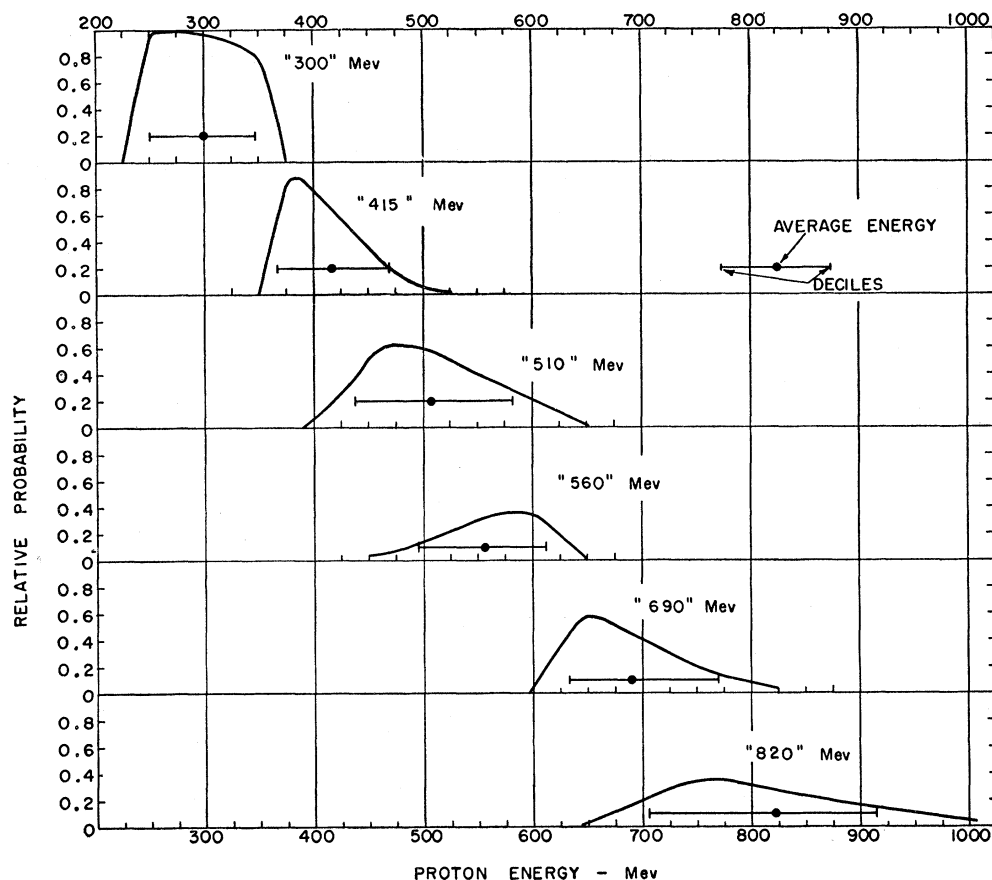
FIG. 5. Calculated distribution of energies within the various selected proton energy groups.

It is possible to calculate the amount of the muon contamination of this group from the data of Table III if an estimate can be made of the ratio of muon fluxes at the two stations. This is less straightforward than the estimation of the proton flux ratio since the variation of muon flux with altitude is somewhat energy-dependent, especially towards the low energy end of the spectrum. Thus, while the flux of slow muons increases by a factor nearly 4[19] between Deep River and Echo Lake, the total flux of all energies increases only by a factor about 2.[20] We expect that in the present experiment the most likely contaminant of the selected proton beam will be the muon flux corresponding to ranges greater than the thickness of material contained in the telescope proper, which is about 145 g cm^{-2} Pb equivalent ($\sim$13 cm Pb). It will therefore be a good approximation to consider the fluxes of single particles as measured under 15-cm lead. At sea level, and at 50°N, Rossi[19] gives the vertical flux under 15-cm lead (essentially all muons) as 0.83×10^{-2} cm^{-2} sec^{-1} sr^{-1}. At 3250 m (690 g cm^{-2} air) altitude we can interpolate between data given for different thicknesses

of lead by Neher[21] to obtain a value 1.74×10^{-2} cm^{-2} sec^{-1} sr^{-1}.[22] This, however, must be corrected for a significant admixture of protons (protons of all ranges >15 cm Pb constitute 10–20% of the penetrating component at this altitude) and we conclude that the ratio of the muon flux at Echo Lake to that at Deep River is between 1.7 and 1.9. This result is consistent with a curve given by Puppi[20] for the total muon flux.

It appears, therefore, that the muon/proton ratio increases in going from Echo Lake to Deep River by a factor between 5 and 6. The work of Conversi[23] on latitude effects, although done at an altitude of 9150 m, implies that the geomagnetic latitude difference between Echo Lake ($\lambda = 49°$N) and Deep River ($\lambda = 58°$N) could not affect the above factor by more than a few percent. It will therefore be assumed that

$$\frac{j_\mu(\text{D.R.})}{j_p(\text{D.R.})} \bigg/ \frac{j_\mu(\text{E.L.})}{j_p(\text{E.L.})} \equiv \frac{r(\text{D.R.})}{r(\text{E.L.})} = 5.5 \pm 0.5, \quad (3)$$

[19] See B. Rossi, Revs. Modern Phys. 20, 537 (1948).

[20] See for example, G. Puppi, Progress in Cosmic-Ray Physics, edited by J. G. Wilson (North Holland Publishing Company, New York, 1956), chap. IV, Vol. III.

[21] H. V. Neher, Progress in Cosmic-Ray Physics, edited by J. G. Wilson (North Holland Publishing Company, New York, 1952), chap. V.

[22] The ratio of the 4-fold coincidence rates at Echo Lake and Deep River due to all particles traversing the telescope in our experiment was 2.0±0.1, which is in good agreement with the ratio 1.74/0.83 = 2.1 given by these quoted fluxes.

[23] M. Conversi, Phys. Rev. 79, 749 (1950).

TABLE III. Ratios of selected proton rates at Echo Lake to those at Deep River.

Energy group (Mev)	200	300	415	510	560	690	820
$\left[\dfrac{\text{(E.L. rate)}}{\text{(D.R. rate)}}\right]$	10.44 ±0.18	10.10 ±0.15	11.13 ±0.25	10.29 ±0.23	9.75 ±0.31	12.15 ±0.25	5.53 ±0.09

where j_p and j_μ are the fluxes in any one energy channel of the telescope of protons and contaminating muons, respectively, and r is the muon/proton ratio in that channel.

From Table III the mean value for the 560 and 690-Mev proton groups gives

$$j_p(\text{E.L.})/j_p(\text{D.R.})=11\pm1, \qquad (4)$$

on the assumption that the meson contamination of these groups is negligible. The value for the 820-Mev group gives

$$\frac{j_p(\text{E.L.})+j_\mu(\text{E.L.})}{j_p(\text{D.R.})+j_\mu(\text{D.R.})}=5.53\pm0.09. \qquad (5)$$

From (3), (4), and (5):

$$\frac{1+r(\text{E.L.})}{1+5.5r(\text{E.L.})}=\frac{5.53}{11},$$

whence $r(\text{E.L.})=0.28\pm0.08$, where the error is mainly due to the $\pm9\%$ uncertainty in the experimental value of $j_p(\text{E.L.})/j_p(\text{D.R.})$.

The effect of this contamination on the interpretation of the neutron data will be considered in Sec. 5.3.

3.3 Calibration of the Neutron Detector

(a) Efficiencies for Neutrons from Calibrated Sources

It can be assumed[24] that the mean energy of the neutrons produced by the protons is bracketed by the mean energies of the neutrons from two available calibrated neutron sources; a Pu^{240} spontaneous fission source, which emits neutrons having an approximately Maxwellian energy distribution with a mean energy of 1.9 Mev,[25] and a Ra-α-Be source which gives neutrons with a wide range of energies 0 to 13 Mev, with a broad maximum at about 4 Mev and a mean energy of ~5 Mev. The principal measurements of the efficiency of the neutron detector were made with these two sources; a 1.5-cm diam sphere of plutonium metal containing about 30% Pu^{240}, having a neutron emission rate of

---

[24] Experimental justification of this assumption is given in Sec. 5.4.

[25] Calculated from Terrell's relation [J. Terrell, Phys. Rev. 113, 527 (1959)]. $\bar{E}=0.78+0.62(\bar{\nu}+1)^{\frac{1}{2}}$ with $\bar{\nu}=2.26$ [B. C. Diven, H. C. Martin, R. F. Taschek, and J. Terrell, Phys. Rev. 101, 1012 (1956)]. [D. W. Colvin and M. G. Sowerby, Proceedings of the Second United Nations International Conference on the Peaceful Uses of Atomic Energy, Geneva, 1958 (United Nations, Geneva, 1958), Paper P/52.] $E_p=\bar{E}/3=T/2$.

8580 ± 130/second, and a Ra-α-Be source of strength $(2.87\pm0.03)\times10^5$/second.

The efficiencies of the different rows of the neutron block were measured for a number of different source positions throughout the target volume, and in the presence of various portions of the target materials placed above and below the plane of the source, in order to take into account the scattering of neutrons by the targets and the secondary fission effect of the uranium target. The effective efficiency for an extended source having the same spatial distribution as that of the disintegration neutrons produced in the targets was then calculated by integrating the product of the measured efficiency and the calculated relative proton interaction density over the volume of the target.

Less detailed measurements were also made using a RdTh-γ-Be source yielding monokinetic neutrons of 0.88-Mev energy, the strength of which was known to
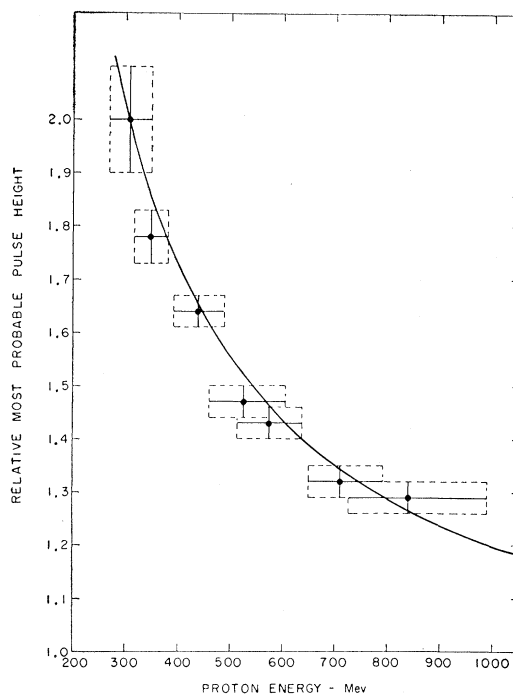

FIG. 6. Observed variation with proton energy of the most probable pulse height in the liquid scintillator. The experimental points are plotted at the average energy of each proton energy group; the energy limits shown are the upper and lower deciles of the energy distributions within each energy group. Most probable pulse heights are measured relative to that observed for fast muons. The solid curve shows the theoretical most probable energy loss as calculated by Millar, Hincks, and Hanna (see reference 17).

TABLE IV. Neutron detection efficiencies for various
rows of neutron counters.[a]

Source	RdTh-γ-Be	Pu spont. fiss.	Ra-α-Be
A row efficiency (%):			
22 g cm^{-2} U target	5.00	5.92	5.00
44 g cm^{-2} U target	5.45	6.45	5.44
Other targets	4.63	5.48	4.63
B row efficiency (%):			
22 g cm^{-2} U target	1.43	2.22	2.27
44 g cm^{-2} U target	1.51	2.35	2.40
Other targets	1.32	2.05	2.09
Σ(C−H) efficiency (%)	0	0.15	0.28

[a] These numbers are of high statistical accuracy, but are subject to the uncertainties in the absolute strengths of the calibrating sources, and to some small errors in the procedure of integration over the target volume.

±10%. The detection efficiencies for the various rows of neutron counters are summarized in Table IV.

The highest total efficiency was obtained with the spontaneous fission source; neutrons from the Ra-α-Be source were detected with a relative efficiency of 0.91, and the 0.88-Mev neutrons with a relative efficiency of 0.78. The enhancement of the efficiency by secondary fission in the 44 g cm^{-2} U target amounted to nearly 20%.

(b) Neutron Lifetime in the Detector

The neutrons produced by proton interactions were recorded only during an interval of 150 microseconds, and it was therefore necessary to measure what fraction of the neutrons were detected during this "gate" interval, i.e., what the "gate efficiency" was. A Pu^{239}-α-Be source provided ($\sim$5 Mev) neutrons in coincidence with 4.43-Mev gamma rays from the reaction Be^9+$\alpha \rightarrow$ C^{12} +n+γ, and the gamma rays, detected in a sodium iodide scintillation counter, triggered two neutron recording systems with gate intervals of 100 and 200 microseconds, respectively. A comparison of the number of counts recorded in the two systems gave, with the assumption of purely exponential decay, "lifetimes" of 144 and 212 microseconds for the counters of the *A* and *B* rows, respectively, leading to preliminary values of the gate efficiencies of 0.62$_5$ and 0.49$_5$, respectively, for a 150 microsecond gate delayed by 5 microseconds. The lifetime, measured by a neutron-neutron coincidence method, was found to be 155 microseconds for the *C* and *D* rows, and 140 microseconds for the lower rows.

The expected lifetime in a large block of paraffin wax is 173±2 microseconds; in the actual block it is reduced by leakage out of the block and absorption by the counters. The lifetime measured by an individual counter will be further influenced by whether (as in the *A* row) there is a net diffusion of slow neutrons away from it to regions of lower density, or (as in the *B* row) towards it from regions of higher density. The first effect does not result in a serious departure from exponential decay, but the second does, with an initially

slower decay. The measured "lifetimes" qualitatively show these effects.

Thus the assumption of purely exponential decay leads to an appreciable error in the calculation of the gate efficiency. The necessary corrections to the gate efficiency were estimated by assuming that the decay could be represented by the sum of a short-lived component and an exponential decay of lifetime 160±10 microseconds. Then, if the short-lived component has entirely decayed in 100 microseconds (the length of the first measuring gate), the measured lifetimes of 144 and 212 microseconds for the *A* and *B* rows indicate corrections of, respectively, −4.2±2.6% and +12.6 ±2.7%, to the gate efficiencies calculated above.[26] For a lifetime of 40 microseconds for the shortlived component, the corrections would be −3.8% and +11.8%; for one of 80 microseconds, they would be −2.2% and 10.2%. Corrections of −2±2% and +11±3% were adopted for the gate efficiencies of the *A* and *B* rows.

The spectrum difference between the proton interaction neutrons and the Pu-α-Be neutrons used in the lifetime measurement is not expected to have any serious effect, but it has been taken into account by increasing the errors in the gate efficiency corrections; this gives corrections of −2±3% for the *A* row and +11±4% for the *B* row. The final gate efficiencies are 0.61±0.02 and 0.55±0.02 for the *A* and *B* rows, respectively. Corrections to the gate efficiencies for the lower rows, which contribute only a few percent of the total neutron detection efficiency may be ignored.

It should be noted that the corrections to the gate efficiency affect the total neutron detection efficiencies by only +2%, since the corrections for the *A* and *B* rows tend to cancel. The effect on the *B/A* ratio (see Sec. 5.4) is $\sim$13%.

4. DESCRIPTION OF TARGETS AND RUNS

In Table V are listed the target materials that were used and their thicknesses. With the exception of tungsten all targets were built up out of machined bars of metal. The tungsten was in powder form and was contained in thin-walled aluminum boxes. Since the ratio of the thicknesses (g cm^{-2}) of aluminum to tungsten in the proton "beam" was only $\sim$0.03, and since the neutron production per gram of aluminum is much less than that for tungsten, the contribution from the boxes may be neglected. In order to help to shield the Geiger counters from the γ rays from the uranium target, and so extend the life of the counters, a peripheral section of the top of each uranium target was replaced by lead. Again, no correction was required for inhomogeneity of the target since the lead not only

<hr>

[26] This discussion applies when there is no delay in starting the gate intervals. In fact the 150 μsecond gate used in the neutron-production measurements and the 100 and 200 μsecond gates of the lifetime measurement were all delayed by 5 μseconds. Unless there is a very short-lived component this does not appreciably change the values of the corrections to be applied.

TABLE V. List of targets.

Element	Atomic weight A	Thickness (g cm^{-2})	Total mass (kg)
Sn	119	22.1	51.5
Sn	119	39.3	91.5
W	184	34.4	82.5
Pb	207	22.1	51.5
Pb	207	44.2	103.0
U	238	22.1	51.5
U	238	44.2	103.0

represented a small fraction of the total target mass, but it was situated on the fringe of the proton "beam" and so was exposed to a small fraction of the total flux.

Because of the low statistical accuracy of the data obtained with the tin targets, the results for the two thicknesses were combined and will be quoted for a mean thickness of 33 g cm^{-2} obtained by weighting the individual thicknesses by the corresponding numbers of recorded protons.

In order to enhance the reliability of the results for the relative neutron production in different targets a program of cycling targets was adopted. During the first part of the experiment, when our main interest was in comparing lead and uranium, runs were made alternating the 44 g cm^{-2} lead and uranium targets. During the second part all the remaining targets listed in Table V were cycled. Runs with no target were interspersed between runs with targets to determine the coherent background (see Sec. 5), and for each group of runs analyzed a background determined from the "no target runs" made during the same period of time was used.

A full series of measurements on all targets was made at Echo Lake. The subsidiary measurements at Deep River, which were used to estimate the muon contamination, were made on the thicker lead and uranium targets only.

5. RESULTS

5.1 The Basic Data and Corrections

For a given sample of data, selected by target and by proton energy, the following basic numbers are obtained from the recorded data: P_e—the number of proton events; N_e—the number of neutron events; and N—the number of detected neutrons.

In order to keep the contamination of the protons by spurious events small we have defined (see Sec. 3) as proton events only those events which satisfy the most rigorous criteria that can be imposed with the Čerenkov and scintillation counter information. The neutron events are those proton events in which one or more neutrons are recorded. The number of detected neutrons is the total number of counts recorded in the neutron events by all BF$_3$ counters.

The mean detected neutron multiplicity per proton event is

$$n = N/P_e, \tag{6}$$

and the mean detected neutron multiplicity per neutron event is

$$t = N/N_e. \tag{7}$$

Before the actual number of neutrons emitted from the target can be calculated several corrections are required. These are, in the order in which they are made: (1) correction for loss of counts by the neutron detection system (counting loss), (2) correction for chance detected neutrons (incoherent background), and (3) correction for neutrons associated with proton events but not produced in the target (coherent background). We shall consider them in turn.

(a) Counting Loss

This correction arises because a single channel of the neutron detection circuit does not record more than one count for each master pulse, even if the BF$_3$ counter or counters to which it is connected have detected two or more neutrons. Since the number of detected neutrons in a single event is occasionally as high as 5 or more and since most of these are recorded in the 6 channels of the A row, there is a significant probability that two or more neutrons fall in the same channel. The magnitude of the loss was determined experimentally in a series of runs in which an auxiliary circuit was operated. This circuit recorded independently, with negligible loss, the total number of neutrons in all channels for each event, and a comparison with the sum of the individual channel counts gives directly ΔN, the number lost. The fractional loss depends upon t, the mean multiplicity of the detected neutrons per neutron event, and the following empirical relation[27] was found to hold over the range of values of $t (1 \leq t \leq 1.6)$ in which we are interested:

$$\Delta N/N = 0.14(t-1). \tag{8}$$

The maximum correction that was made for counting loss was thus about 8%.

(b) Incoherent Background

The number of chance neutrons recorded in each neutron gate opening is given by the product of the ungated neutron counting rate, R, and the gate width, τ. Since the time distribution of the ungated neutrons is very nearly random and the probability of a chance count is low, chance neutron events with multiplicities greater than unity can be neglected. The ungated neutron rate was monitored throughout each run, and the gate width (150 microseconds) was checked several times during the experiment. Only in the case of the

---

[27] The proportionality of the fractional loss to $(t-1)$ may be deduced theoretically for the special case of an exponential distribution of recorded multiplicities, i.e., $N_e(x) \propto \exp(-x/x_0)$ where $N_e(x)$ is the number of events in which $x(>0)$ neutrons are detected. An exponential distribution was in fact observed to hold, within statistical uncertainty, for every sample representing a particular target and a particular proton energy.

uranium targets which produce a large background of spontaneous fission neutrons was the chance rate appreciable. With the thickest U target and at the lowest proton energy the correction approached 20% of the total number of detected neutrons.

The values of n and t including the corrections for counting loss and incoherent background will be called n' and t':

$$n' = \frac{N[1+0.14(t-1)]-R\tau P_e}{P_e} \equiv \frac{N'}{P_e}, \qquad (9)$$

$$t' = \frac{N[1+0.14(t-1)]-R\tau P_e}{N_e - R\tau P_e} \equiv \frac{N'}{N_e'}. \qquad (10)$$

The error in n' is determined by first estimating the statistical uncertainty in N. Due to the occurrence of multiplicities greater than unity, $\sigma(N)$, the standard deviation of N, will be in general larger than $N^{\frac{1}{2}}$. For an exponential multiplicity distribution[27] and for values of t that are not too large it can easily be shown that $\sigma(N)$ is given quite accurately by

$$\sigma(N) = tN^{\frac{1}{2}}. \qquad (11)$$

The corrections for counting loss and incoherent background introduce negligible additional uncertainty so that the standard deviation of n' is, from (9) and (11),

$$\sigma(n') = tN^{\frac{1}{2}}[1+0.14(t-1)]/P_e. \qquad (12)$$

It may be shown that the standard deviation of t, again for an exponential multiplicity distribution and t not too large, is

$$\sigma(t) = [t(t=1)/N]^{\frac{1}{2}}. \qquad (13)$$

The complete expression for $\sigma(t')$ is rather complicated, but the following approximation based on Eq. (13) and the condition $R\tau P_e \ll N_e$ is sufficiently accurate for our use;

$$\sigma(t') = \left[\frac{t(t-1)}{N} \left(1 + \frac{2R\tau P_e}{N_e} \right) \right]^{\frac{1}{2}}. \qquad (14)$$

(c) Coherent Background

The most difficult correction to determine exactly is that for background neutrons associated with the selected protons but not produced in the target. Some of these neutrons will be produced by protons which, having traversed the target, interact in the material below (paraffin and counter walls).Others may originate in materials above the target, for example, in the lead absorber, provided of course, that a charged particle penetrates far enough to ensure the generation of a master pulse. This background is measured in runs with the target removed but then must be adjusted to allow for the influence of the target upon it. If a fraction, f, of the protons interact in the target, the portion of the background originating below the target position will evidently be reduced by a factor of at most $(1-f)$, the proton attenuation in the target. Any neutrons origi-

nating from above the target will probably be little attenuated.

Therefore, the factor k by which the coherent background measured in the "no target runs" should be multiplied to allow for the presence of a target lies between 1 and $(1-f)$, so, lacking better information, we shall use the central value and limits of error given by

$$k = (1-f/2) \pm f/2. \qquad (15)$$

The largest proton absorption calculated from accepted cross-section data in any of the targets used is 20%, so that the greatest uncertainty in any value of k is 11%.

The mean detected neutron multiplicity per proton, [Eq. (9)], when fully corrected for counting loss and background, is denoted by m,

$$m = n_T' - kn_0', \qquad (16)$$

where the subscripts T and 0 refer to values of n' obtained with and without a target, respectively. The error in m is obtained by adding linearly the fractional uncertainty in k to that in n_0', and then adding the errors in n_T' and kn_0' in quadrature. The coherent background correction is an important one; the magnitude of kn_0' ranges from 10 to 50% of that of n_T', depending upon the target and the proton energy.

Similarly, the mean detected neutron multiplicity per neutron event, [Eq. (10)], when fully corrected is denoted by s,

$$s = \frac{n_T' - kn_0'}{n_T'/t_T' - kn_0'/t_0'}. \qquad (17)$$

The errors that have been tabulated for s slightly underestimate the true errors since the inclusion (in quadrature) of the error in kn_0' has been omitted.

5.2 Values of n', t', m, and s

Following the procedures described in section (a) values of n', t', m, and s were calculated and are presented in Tables VI, VII, VIII, and IX, respectively. The various columns are for proton groups of different mean energies. Neutron data were not computed for the lowest energy proton group selected (from 0 to ~ 250 Mev) since a large fraction of this group would have ranges less than the target thickness and the results would not be very meaningful.

Tables VI, VII, VIII, and IX contain the results of all the final Echo Lake and Deep River runs. It will be noted in Tables VI and VII that two different sets of "no target" data are given for Echo Lake. That marked (a) was measured during the period in which the Sn, W, Pb(22), and U(22) targets were studied, and furnishes the background appropriate to them; that marked (b) was measured during the period in which the Pb(44) and U(44) targets were studied. Table VIII gives, in addition to m, the values of k that were used to make the coherent background correction.

TABLE VI. Values of n', the mean number of detected neutrons per incident proton, corrected for counting loss and incoherent background, for Echo Lake (E.L.) and Deep River (D.R.) runs.

Location of runs	Target: element and thickness (g cm^{-2})	Mean energy of proton group (Mev)					
		300	415	510	560	690	820
E.L.	None (a)	0.012±0.002	0.027±0.005	0.030±0.005	0.033±0.007	0.044±0.005	0.037±0.005
E.L.	None (b)	0.016±0.003	0.021±0.005	0.027±0.006	0.048±0.011	0.038±0.006	0.037±0.006
E.L.	Sn (33)	0.052±0.005	0.068±0.009	0.079±0.010	0.089±0.015	0.099±0.009	0.100±0.010
E.L.	W (34)	0.051±0.006	0.110±0.016	0.104±0.015	0.085±0.017	0.144±0.014	0.130±0.015
E.L.	Pb (22)	0.049±0.004	0.083±0.008	0.066±0.007	0.063±0.009	0.097±0.008	0.088±0.007
E.L.	Pb (44)	0.084±0.006	0.119±0.010	0.131±0.011	0.180±0.019	0.155±0.010	0.178±0.012
E.L.	U (22)	0.070±0.006	0.095±0.010	0.099±0.010	0.120±0.016	0.104±0.009	0.111±0.010
E.L.	U (44)	0.130±0.008	0.204±0.016	0.207±0.016	0.214±0.024	0.260±0.018	0.246±0.018
D.R.	None	0.018±0.004	0.018±0.006	0.017±0.005	0.007±0.005	0.033±0.007	0.016±0.004
D.R.	Pb (44)	0.078±0.007	0.121±0.013	0.102±0.014	0.130±0.023	0.136±0.015	0.091±0.008
D.R.	U (44)	0.146±0.013	0.184±0.022	0.162±0.022	0.195±0.040	0.211±0.026	0.112±0.012

TABLE VII. Values of t', the mean number of detected neutrons per neutron event, corrected for counting loss and incoherent background, for Echo Lake (E.L.) and Deep River (D.R.) runs.

Location of runs	Target: element and thickness (g cm^{-2})	Mean energy of proton group (Mev)					
		300	415	510	560	690	820
E.L.	None (a)	$1.03^{+0.07}_{-0.03}$	$1.00^{+0.06}_{-0.00}$	$1.02^{+0.06}_{-0.02}$	$1.00^{+0.10}_{-0.00}$	$1.09^{+0.04}_{-0.03}$	$1.03^{+0.05}_{-0.03}$
E.L.	None (b)	$1.03^{+0.09}_{-0.03}$	$1.05^{+0.12}_{-0.05}$	$1.00^{+0.09}_{-0.00}$	$1.00^{+0.10}_{-0.00}$	$1.15^{+0.06}_{-0.05}$	$1.11^{+0.07}_{-0.05}$
E.L.	Sn (33)	1.15±0.03	1.14±0.04	1.15±0.04	1.15±0.06	1.19±0.04	1.27±0.05
E.L.	W (34)	1.21±0.05	1.41±0.07	1.42±0.07	1.22±0.08	1.30±0.04	1.37±0.06
E.L.	Pb (22)	1.22±0.03	1.30±0.04	1.17±0.03	1.18±0.05	1.31±0.04	1.29±0.04
E.L.	Pb (44)	1.26±0.03	1.30±0.04	1.38±0.04	1.43±0.05	1.38±0.03	1.46±0.04
E.L.	U (22)	1.35±0.04	1.40±0.05	1.37±0.05	1.33±0.06	1.25±0.03	1.43±0.05
E.L.	U (44)	1.46±0.03	1.59±0.04	1.56±0.04	1.60±0.06	1.81±0.04	1.81±0.05
D.R.	None	$1.00^{+0.11}_{-0.00}$	$1.00^{+0.26}_{-0.00}$	$1.00^{+0.23}_{-0.00}$	$1.0^{+1.2}_{-0.0}$	$1.00^{+0.11}_{-0.00}$	$1.00^{+0.12}_{-0.00}$
D.R.	Pb (44)	1.16±0.03	1.26±0.05	1.40±0.07	1.49±0.09	1.37±0.05	1.31±0.04
D.R.	U (44)	1.48±0.04	1.55±0.07	1.63±0.08	2.07±0.14	1.94±0.08	1.62±0.06

TABLE VIII. Values of m, the mean number of detected neutrons per incident proton, corrected for counting loss, incoherent background, and coherent background. Echo Lake (E.L.) and Deep River (D.R.) runs.

Location of runs	Target: element and thickness (g cm^{-2})	Factor k used to correct no target background	Mean energy of proton group (Mev)					
			300	415	510	560	690	820
E.L.	Sn (33)	0.91	0.041±0.006	0.043±0.011	0.052±0.012	0.059±0.018	0.059±0.012	0.066±0.013
E.L.	W (34)	0.92	0.040±0.007	0.085±0.018	0.076±0.017	0.055±0.019	0.104±0.017	0.096±0.018
E.L.	Pb (22)	0.95	0.038±0.004	0.057±0.010	0.038±0.010	0.032±0.012	0.055±0.010	0.053±0.010
E.L.	Pb (44)	0.90	0.070±0.008	0.100+0.012	0.107±0.013	0.137±0.025	0.121±0.013	0.145±0.015
E.L.	U (22)	0.95	0.059±0.006	0.069±0.012	0.071±0.012	0.089±0.018	0.062±0.011	0.076±0.012
E.L.	U (44)	0.90	0.116±0.010	0.185±0.018	0.183±0.018	0.171±0.029	0.226±0.021	0.213±0.021
D.R.	Pb (44)	0.90	0.062±0.009	0.105±0.015	0.087±0.016	0.124±0.023	0.106±0.018	0.077±0.010
D.R.	U (44)	0.90	0.130±0.015	0.168±0.024	0.147±0.023	0.189±0.040	0.181±0.029	0.098±0.014

5.3 Muon Contamination Correction

We may compare directly, see Table X, the values of m obtained for the Pb(44) and U(44) targets at Echo Lake with those obtained at Deep River. The ratios of the measured values, m(Deep River)$/m$(Echo Lake), are listed. These ratios are quite insensitive to the values of k used and the errors shown are due almost entirely to the errors in the values of n_T'.

Table X shows that there is a marked drop in the value of m(D.R.)$/m$(E.L.) in the 820-Mev proton

TABLE IX. Values of s, the mean number of detected neutrons per neutron event, corrected for counting loss, incoherent background, and coherent background. Echo Lake (E.L.) and Deep River (D. R.) runs.

Location of runs	Target: element and thickness (g cm⁻²)	Mean energy of proton group (Mev)					
		300	415	510	560	690	820
E.L.	Sn (33)	1.20±0.04	1.22±0.07	1.24±0.06	1.26±0.10	1.26±0.07	1.44±0.09
E.L.	W (34)	1.29±0.07	1.60±0.10	1.68±0.11	1.38±0.14	1.39±0.06	1.55±0.09
E.L.	Pb (22)	1.31±0.04	1.50±0.07	1.32±0.06	1.45±0.12	1.53±0.08	1.56±0.08
E.L.	Pb (44)	1.32±0.04	1.35±0.05	1.50±0.05	1.65±0.08	1.47±0.04	1.58±0.05
E.L.	U (22)	1.44±0.05	1.64±0.08	1.59±0.08	1.51±0.09	1.37±0.05	1.73±0.09
E.L.	U (44)	1.55±0.04	1.68±0.05	1.68±0.05	1.88±0.09	1.98±0.05	2.01±0.06
D.R.	Pb (44)	1.21±0.04	1.31±0.06	1.50±0.09	1.53±0.10	1.54±0.07	1.40±0.05
D.R.	U (44)	1.57±0.05	1.63±0.08	1.72±0.10	2.15±0.15	2.29±0.11	1.78±0.08

TABLE X. Values of the ratios m (Deep River)/m (Echo Lake) for the thicker Pb and U targets.

Target				Mean energy of proton group (Mev)		
	300	415	510	560	690	820
Pb (44)	0.89±0.15	1.05±0.18	0.81±0.17	0.91±0.22	0.88±0.15	0.53±0.08
U (44)	1.12±0.15	0.91±0.15	0.80±0.14	1.11±0.29	0.80±0.14	0.46±0.07

energy group due to the muon contamination discussed in Sec. 3.2(b). If nearly all of the contaminating muons are assumed to be fast, and therefore produce a negligible number of neutrons,[28] the muon contamination reduces m directly, and the correction factors for the 820-Mev group at Echo Lake and at Deep River are simply [1+r(E.L.)] and [1+r(D.R.)], respectively. Since the corrected values of m at Echo Lake and at Deep River, m(E.L.)[1+r(E.L.)] and m(D.R.)[1+r (D.R.)] must be equal, we would then calculate from Eqs. (4) and (5), that m(D.R.)/m(E.L.)= (5.53±0.09)/ (11±1)=0.50±0.05, which is consistent with the directly measured values of Table X.

On the other hand, if an appreciable number of muons stop in the target and undergo nuclear capture, the neutron contribution of the muons could be significant. Whereas the proportion of all muons passing through the telescope which stop in the target is only 2%, the Čerenkov selection, by discriminating against high particle velocities, probably enhances this proportion. However, from the errors in the measured and calculated values of m(D.R.)/m(E.L.) and the ratio of the flux of stopping muons at the two altitudes, known to be ~3.3,[29] we can place an upper limit of 5% on the proportion of muon-produced neutrons at Echo Lake, and 15% at Deep River.[30] In correcting the 820-Mev

Echo Lake values of m the correction factor of 1.28 ±0.08 from Sec. 3.2(b) has been rounded off to 1.3 ±0.1, and the error has been added linearly to the uncertainty in m.

There is also some indication that the Deep River m values for the 510 Mev and 690-Mev proton groups are lower than the Echo Lake values. However, the hypothesis of a muon contamination in these groups is not borne out by the relative proton flux figures given in Table III and it will be assumed that the Echo Lake figures are reliable.

Further analysis will be based on the Echo Lake results only.

5.4 The Neutron Energies: Penetration in the Paraffin Block

(a) The Detection Efficiency or Neutrons from the Targets

We must now see to what extent the experimental data justify our assumption that the efficiency of the neutron detection assembly for neutrons from all targets and all proton energies lies between the efficiencies for Pu spontaneous fission and Ra-α-Be neutrons. The validity of the assumption is governed by the relationship between the neutron energy spectra. A rough criterion of the effective mean energy of the neutrons emitted from the targets is given by the rate of attenuation of thermal neutron density with depth in the moderator.

We shall use as a measure of the neutron penetration the ratio "B/A," that is the ratio of the number of neutrons detected in the B row of counters to the number detected in the A row. The corrections that

---

[28] B. F. Stearns, D. R. Jones, J. K. de Pagter, and R. D. Sard Phys. Rev. **106**, 1043 (1957), have measured a value $(\sigma_a \nu)_\mu$=2.2 ×10⁻²⁸ neutrons cm²/nucleon in lead, or 5×10⁻²⁶ neutrons cm²/ lead nucleus. By comparison, the results of this experiment show that for protons in the energy range of interest, $(\sigma_a \nu)_p$~10⁻²³ neutrons cm²/lead nucleus.

[29] See G. Puppi and N. Dallaporta, *Progress in Cosmic-Ray Physics* edited by J. G. Wilson (North Holland Publishing Company, New York, 1952), chap. VI. p. 340.

[30] If the muons produce no neutrons then they will not affect the values of t' or s. A comparison of the observed values of s at

Echo Lake and Deep River (Table IX) suggests that the values of s(D.R.) are perhaps 10 to 20% smaller at 820 Mev.

were made to the raw data are similar to those that were made in deriving the value of m. The backgrounds, both incoherent and coherent, were calculated in a straightforward manner. The loss due to channel dead-time was estimated in a semiempirical way by dividing the total loss, used for m, between the A and B rows, in a way depending upon the relative multiplicities observed in each separately. It turned out that between 90 and 95% of the total loss could be attributed to the A row.

To make the observed B/A ratios comparable with those found from the ungated measurements with the calibrating neutron sources a correction was also made for the difference in the neutron gate efficiencies between the A and B rows of counters. The correction factor for this effect is 1.11 ± 0.05.

Corrected values of B/A for the various targets are given in Table XI along with the values observed for the three calibrating sources. The 300, 415, and 510-Mev proton data have been added together under the heading "low E_p," and the 560, 690, and 820-Mev data are combined under "high E_p." There is, in fact, no evidence of a systematic variation in the value of B/A with proton energy. Thus, combining the data for all targets we find

$$\frac{(B/A)_{\text{high } E_p}}{(B/A)_{\text{low } E_p}} = 0.93\pm0.08, \qquad (18)$$

which is not significantly different from unity.

We shall therefore confine our attention to the column labelled "Total" in which all data for a given target are combined. There appears to be a significant difference between B/A values for the lead (averaged for the 22 and 44 g cm^{-2} thicknesses), tungsten, and tin targets on the one hand, none of which is inconsistent with the Ra-α-Be value of 0.45; and on the other hand, the B/A value averaged for the uranium 22 and 44 g cm^{-2} targets which lies close to the plutonium spontaneous fission values of 0.37. This leads us to adopt the measured efficiency for the spontaneous fission neutrons as appropriate for the neutrons emitted from the uranium targets, and the measured efficiency for the Ra-α-Be neutrons as appropriate for neutrons emitted from the other targets. Using the neutron efficiency values of Table IV, and the corrected gate efficiencies quoted in Sec. 3.3, we arrive at the following total gated neutron efficiencies; 5.0% and 5.4% for the 22 and 44 g cm^{-2} uranium targets, respectively, and 4.2% for all other targets.

(b) Systematic Variations of B/A with Target

In addition to the difference between the B/A values found for the uranium targets and the values found for the other targets, there is also evidence that B/A decreases with increasing target thickness. Thus combining the data of Table XI for lead and uranium,

TABLE XI. Values of the ratio B/A, the relative numbers detected in the B and A rows of BF$_3$ counters for the various targets and for the neutron sources used for calibration.

Target or neutron source	Low E_p	High E_p	Total
Sn (33)	0.50±0.11	0.46±0.11	0.48±0.08
W (34)	0.52±0.11	0.38±0.08	0.44±0.07
Pb (22)	0.53±0.10	0.51±0.11	0.52±0.07
Pb (44)	0.40±0.05	0.40±0.06	0.40±0.04
U (22)	0.39±0.07	0.37±0.08	0.38±0.05
U (44)	0.34±0.04	0.32±0.04	0.33±0.03
RdTh-γ-Be			0.28
Pu spontaneous fission			0.37±0.01
Ra-α-Be			0.45

we find

$$\frac{(B/A)_{22 \text{ g cm}^{-2} \text{ target}}}{(B/A)_{44 \text{ g cm}^{-2} \text{ target}}} = 1.22\pm0.12. \qquad (19)$$

These variations are to be ascribed largely to secondary processes within the targets.

In the case of the 44 g cm^{-2} uranium target, the observed enhancement of the neutron detection efficiency due to secondary fission implies that $\sim20\%$ of the low-energy neutrons emerging from the target arise from this process. When we include fission in the primary interaction, which produces about two extra neutrons near the end of the evaporation chain (see Sec. 6.1) we conclude that between one quarter and one third of all neutrons detected from the thick uranium target originate in low-energy fission processes. Since the mean energy of the fission spectrum is lower than that of the evaporation spectrum, we may expect a lowered mean energy for neutrons emerging from the target and therefore a lowered B/A ratio. This effect is obviously larger for thicker targets.

Again, in all targets, secondary interactions by cascade nucleons may be expected to yield evaporation neutrons lower in energy than those arising from the primary interactions of the incident protons, since the much lower energy of the cascade nucleons produces smaller average nuclear excitations. The lowering of average energy of the detected neutrons is greatest where the ratio of the numbers of secondary interaction neutrons to primary interaction neutrons is greatest. The calculated number of secondary neutrons per primary interaction seen in Table XV shows this ratio to increase with target thickness, atomic weight, and incident proton energy.

Further, at energies of the order of 10–20 Mev, the neutron detection efficiency is not entirely negligible, and low-energy cascade neutrons may themselves be directly detected, making B/A higher than would be expected for a pure evaporation spectrum. At a given incident proton energy, the ratio of cascade neutrons to evaporation neutrons increases with decreasing

TABLE XII. Values of μ, the mean number of neutrons produced per incident proton and per unit thickness of target. Echo Lake data, with the 820-Mev figures corrected for muon contamination.

Target: element and thickness ($g \, cm^{-2}$)	Mean energy of proton group (Mev)					
	300	415	510	560	690	820
Sn (33)	0.028±0.004	0.030±0.007	0.035±0.008	0.041±0.013	0.041±0.008	0.059±0.014
W (34)	0.027±0.004	0.056+0.012	0.050±0.011	0.037±0.013	0.069±0.011	0.083±0.019
Pb (22)	0.040±0.004	0.059±0.011	0.040±0.011	0.033±0.013	0.057±0.011	0.071±0.016
Pb (44)	0.035±0.004	0.051±0.006	0.055±0.006	0.070±0.013	0.061±0.006	0.096±0.015
U (22)	0.051±0.005	0.060±0.011	0.062±0.011	0.077±0.016	0.054±0.010	0.085±0.018
U (44)	0.047±0.004	0.074±0.007	0.073±0.007	0.069±0.012	0.091±0.009	0.112±0.018

atomic weight and this will correspondingly affect the B/A ratio.

The trends observed in the B/A values are qualitatively consistent with all the preceding arguments.

The mean value of B/A for all targets and all energies is 0.43, which is consistent with a mean energy for all detected low-energy neutrons between two and five Mev. Experiments at incident energies between 150 and 200 Mev by Gross,[6] Gol'danskii et al.,[7] Skyrme and Williams,[5] Skyrme and Harding[31] all give mean neutron energies close to 2.5 Mev for a variety of targets between silver and uranium. At a considerably higher energy corresponding to a nuclear excitation energy of 200 Mev in silver, Dostrovsky et al.[4] calculate a mean evaporation neutron energy of $\sim$6 Mev. (From Metropolis et al.[3] we deduce an average nuclear excitation

FIG. 7. The neutron production per gram in the 44 g cm^{-2} targets relative to that in the 22 g cm^{-2} targets for different proton energy groups. Corrections have been made for proton attenuation in the targets.

[31] D. M. Skyrme and G. N. Harding, Nuovo cimento 9, 1082 (1958).

energy of 170 Mev for 820-Mev protons incident on tin.) Thus external evidence yields upper and lower limits to the mean neutron energy consistent with those observed.

5.5 Values of μ, the Neutron Yield per Proton per gram cm^{-2}

The mean number of neutrons emitted per incident proton per unit thickness (g cm^{-2}) of a target of effective thickness T is given by

$$\mu = m/\epsilon T, \qquad (20)$$

where ϵ is the neutron detection efficiency.

In Table XII are given the values of μ calculated from the Echo Lake values of m using Eq. (20) and the efficiencies from Sec. 5. (a). The values of T used were the actual target thicknesses increased by 5% to allow for the mean increase in path length of the protons in the target resulting from their angular spread with respect to the telescope axis. The mean increase in path length was calculated on the basis of the telescope geometry and a cos$^3\theta$ zenith angle dependence of the proton flux.

We are now in a position to compare the results obtained from targets of different thickness (22 g cm^{-2} and 44 g cm^{-2}) of the same element (Pb or U). Assuming only that the neutron spectrum is the same for both thicknesses, but not identifying it with any particular spectrum, the ratio of the values of μ for the two thicknesses will evidently be very close to the ratio of true neutron yields per unit thickness of the two targets. Differences between the values of μ for two different thicknesses of the same target material must then be attributed to one or both of two effects: (a) attenuation of the incident proton beam resulting in a smaller yield from the thicker target, and (b) multiplication by the additional interactions of high-energy secondary nucleons[32] which will give a larger yield from the thicker target. Corrections for attenuation may be readily made. It will be convenient to introduce a quantity q, the mean probability per unit thickness for the inter-
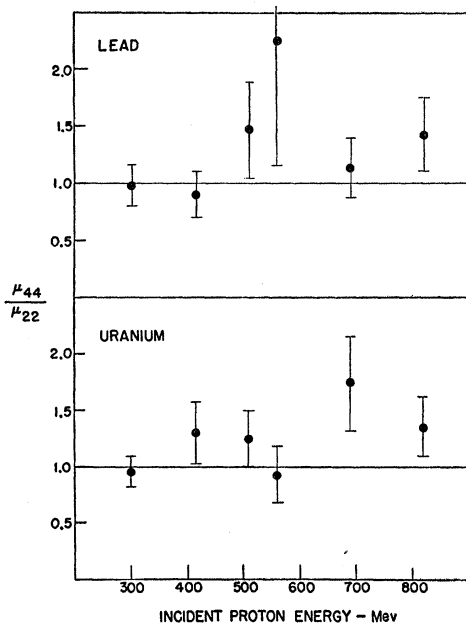
[32] The ordinary "fast fission" contribution in the uranium targets due to neutrons in the Mev region is not included in the values of μ since it is included in the enhancement of the values of ϵ as a result of the method of calibration.

TABLE XIII. Values of ν, the mean number of neutrons produced per interaction, derived from the values of μ and the cross sections given by Chen, Leavitt, and Shapiro.[a] The neutrons arising from multiplication in the various targets are included.

Target: element and thickness (g cm^{-2})	Mean energy of proton group (Mev)					
	300	415	510	560	690	820
Sn (33)	5.8±1.0	6.1±1.5	7.1±1.7	8.1±2.6	8.0±1.7	11.5±2.7
W (34)	6.2±1.0	12.5±2.7	11.1±2.4	7.9±2.8	14.9±2.4	17.6±4.2
Pb (22)	9.2±1.0	13.4±2.5	8.9±2.4	7.4±2.9	12.4±2.4	15.3±3.6
Pb (44)	8.6±1.1	12.2±1.5	12.9±1.5	16.2±3.0	14.0±1.5	22.0±3.4
U (22)	12.4±1.2	14.2±2.6	14.4±2.6	17.9±3.7	12.4±2.3	19.3±4.0
U (44)	12.0±1.0	18.5±1.7	18.0±1.7	16.6±2.9	21.9±2.1	26.7±4.2

[a] See reference 31.

action of an incident proton in a given target.[33] For a "thin target" (attenuation negligible) of thickness T g cm^{-2} we have

$$q = f/T = N\sigma_a/A, \quad (21)$$

where N is Avogadro's number, σ_a is the nuclear interaction cross section, and A is the atomic weight. For a thick target, q depends on the thickness, and we shall write

$$q_T = 1/T[1 - e^{-N\sigma_a T/A}]. \quad (22)$$

Hence, the correction factor required to remove the effect of absorption from the ratio of μ for the 44 g cm^{-2} target to μ for the 22 g cm^{-2} target (μ_{44}/μ_{22}) is[34]

$$\frac{q_{22}}{q_{44}} = 2\left(\frac{1 - e^{-22N\sigma_a/A}}{1 - e^{-44N\sigma_a/A}}\right) - \frac{1 - 11N\sigma_a/A}{1 - 22N\sigma_a/A}. \quad (23)$$

We have used for σ_a data from the compilation by Chen, Leavitt, and Shapiro.[35] The values of $q_T T$, the interaction probability in the whole target, are between 0.09 and 0.10 for the thinner U and Pb targets and between 0.17 and 0.19 for the thicker targets in the range of energies 300 to 820 Mev.

In Fig. 7(a) and (b) are plotted the ratios μ_{44}/μ_{22} for lead and uranium, with the corrections for absorption made as outlined above. Notwithstanding the size of the errors, the trend upwards from unity as the proton energy increases is evidence of an additional multiplication in the 44 g cm^{-2} targets over that in the 22 g cm^{-2} targets. Thus we infer that even the 22 g cm^{-2} targets are thick in the sense that the effect of secondary interactions is appreciable [as already tacitly assumed in Sec. 5.4(b)]. Further discussion of this effect is deferred to Sec. 6.

[33] Elastic scattering may be neglected since it is predominantly in the forward direction.
[34] The 5% increase in the effective value of T due to the angular spread of the incident protons is neglected here, since the effect on the correction factor is only 0.3%.
[35] F. F. Chen, C. P. Leavitt, and A. M. Shapiro, Phys. Rev. 99, 857 (1955). These authors give values for tin and lead. Values for uranium and tungsten were obtained by interpolation using $\sigma_a \propto A^{\frac{2}{3}}$.

5.6 Values of ν, the Mean Neutron Multiplicity per Interaction

Since we do not distinguish with good efficiency in this experiment those protons that interact from those that do not, we cannot determine separately the values of absorption cross section and of neutron multiplicity per interaction. We have calculated values of ν, the mean number of neutrons per interaction, from our values of μ (Table XI) and published[35] nucleon-nucleus cross sections. Thus from (21) we have for a thin target

$$\nu = \mu/q = A\mu/N\sigma_a, \quad (24)$$

and from (22), for a thick target

$$\nu = \mu/q_T = A\mu/N\sigma_a[1 + NT\sigma_a/2A + \cdots]. \quad (25)$$

For all our targets higher terms in the expansion are negligible. For values of ν are given in Table XIII. Note that no correction for neutrons from secondary interactions in the target has yet been made, so that these are included in the quantity ν.

It will be noted that, in general, ν increases with A, and also with E_p, although we cannot say how much of the increase is due to higher multiplicities from the primary interactions and how much is due to an increase in the number of secondary interactions and in their neutron yield. The values of ν lie between ~ 6 for tin at low-proton energy, to > 20 for the heavier targets at high-proton energy. A comparison with results both from other experiments and from theoretical predictions will be made later in Sec. 6.

5.7 Calculation of s from ν: Evidence for a Multiplicity Distribution

If the neutron multiplicity distributions leading to the values of ν given in Table XIII were known, s, the mean number of detected neutrons per neutron event could be calculated and compared with the experimental values presented in Table IX. In the case of a line distribution, where exactly ν neutrons are emitted in each interaction and are detected with an efficiency ϵ, it may be shown that

$$s(\nu) = \epsilon\nu/[1 - (1-\epsilon)^\nu]. \quad (26)$$

TABLE XIV. Values of $\bar{s}$ for various multiplicity distributions. The line distribution value $s(\nu)$ is 1.25 in all cases.

Distribution	ν_{max}	$\bar{\nu}$	$\bar{s}$
(i)	20	10	1.28
(ii)	15	10.33	1.29
(iii)	31	10	1.39

The values of $s(\nu)$ calculated from Eq. (26) using the corrected mean multiplicities given in Table XIII are generally 10–20% lower than the experimental values of s listed in Table IX. This difference may be attributed to the existence of a spread of neutron multiplicities in the primary emission process.

To illustrate this point, the average number of detected neutrons per neutron event, $\bar{s}$, has been calculated for the three simple assumed multiplicity distributions listed below. Each has a mean multiplicity, $\bar{\nu}$, close to 10 and each goes to zero at some maximum value of $\nu = \nu_{max}$.

(i) Rectangular distribution; probability of multiplicity ν is constant for $0 < \nu < \nu_{max}$.

(ii) Triangular distribution; probability of multiplicity ν increases linearly from zero at $\nu = 0$ to a maximum at $\nu = \nu_{max}$.

(iii) Triangular distribution; probability of multiplicity ν decreases linearly from maximum value at $\nu = 0$ to zero at $\nu = \nu_{max}$.

The values of $\bar{s}$ calculated for these distributions, taking $\epsilon = 0.050$, are given in Table XIV and may be compared with $s(\bar{\nu}) = 1.25$, the line distribution value.

It is seen that $\bar{s}$ is relatively insensitive to the shape of the assumed multiplicity distribution and does not differ greatly from $s(\bar{\nu})$ in the two cases where the distribution is approximately symmetric about $\bar{\nu}$, or where ν_{max} is not very much greater than $\bar{\nu}$. In the case of distribution (iii) where there is a high multiplicity tail, $\bar{s}$ exceeds $s(\bar{\nu})$ by 11%, which suggests that the experimental multiplicity distributions are qualitatively closer to distribution (iii) than to (i) or (ii).

The nuclear cascade calculations of Metropolis et al.[3] show that for low energy (below 100 Mev) nucleons incident on heavy nuclei, there is a pronounced peak in the excitation energy distributions near the maximum possible energy, which would lead to neutron multiplicity distributions similar to (ii). At the higher energies involved in this experiment, the excitation energy distributions become Maxwellian in character, with high-energy tails extending to values three or more times the mean excitation energies. In these cases neutron multiplicity distributions qualitatively similar to (iii) would be expected.

5.8 Evidence for High-Energy Neutrons

Since the rate of attenuation of the neutron counting rate with depth in the paraffin moderator decreases with increasing energy, at least up into the hundred Mev region where the scattering cross sections of hydrogen and carbon begin to level off, we may look to the counters that are deeper in the paraffin for evidence for high-energy neutrons.

If we examine the numbers of neutrons counted in the four deepest rows of counters (E, F, G, H) we find that there is no significant increase due to the presence of a target. This is because the incident protons that do not interact in the target, and which are not distinguished experimentally from those which do, produce a relatively large neutron background when they interact with carbon close to the lower counters, or with the materials of the counters themselves. To reduce the relative background we are forced to select from the proton events those in which there is no PC_3-PC_4 coincidence. These are the events in which no charged particle is detected below the target and are mainly interactions without fast secondary protons.

Using these events only, the data for all targets and for all proton energies have been combined to yield the variation of number of detected neutrons with depth shown in Fig. 8. For simplicity the counters have been divided into four groups: Row A, Row B, Rows C, D, and Rows E, F, G, H, and the numbers of counts corrected for background and for differences in gating efficiency are normalized to the number in Row A. Figure 8 also shows for comparison the relative counting rates for each of the three calibrating neutron sources. The horizontal scale is arbitrary; the positions at which the points were plotted were chosen to make the Ra-α-Be points fall on a straight line with 45° slope on the plot. The position of the "proton interaction" points relative to those for the spontaneous fission and Ra-α-Be sources clearly implies that while most of the neutrons from the proton interactions have energies between the mean energies of these two sources, there also exists a high-
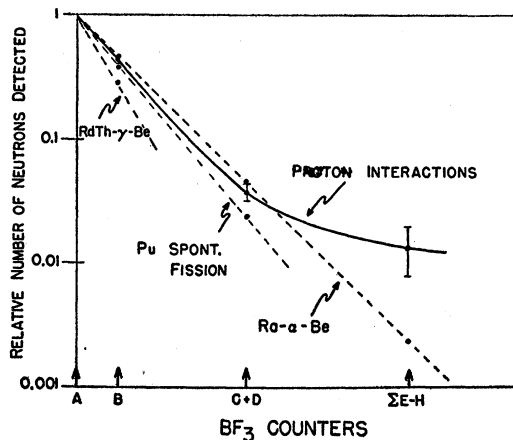

FIG. 8. The relative neutron counting rates in counters at different depths in the paraffin moderator for neutrons from proton interactions, and for neutrons from various calibrating sources. The abscissas are arbitrary (see text).

energy tail which is responsible for the relatively large number of neutrons detected below Row D.

Since the detection efficiency falls off very rapidly as the neutron energy increases above 10 Mev, a very long running time would be required to obtain data of reasonable statistical accuracy from the lower counters. Because of the difficulty in determining the detection efficiency only qualitative indication of the emission of high-energy neutrons in the proton interactions was obtained.

6. DISCUSSION

6.1 Comparison with Theory

To compare our experimental results with theoretical predictions, we have calculated the average numbers of low-energy neutrons expected from the proton bombardment of our targets. We used the Monte Carlo calculations of Metropolis et al.,[3] which give the average excitation energy of the target nuclei for several dif-
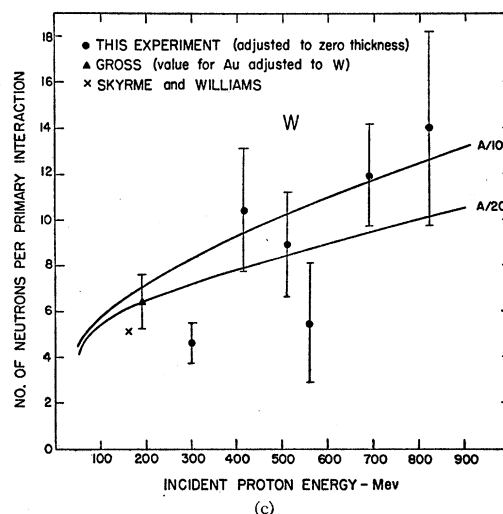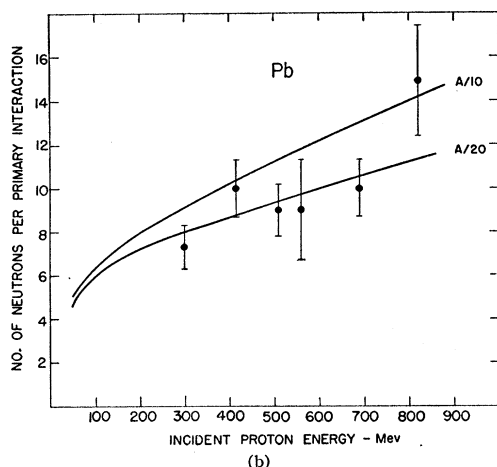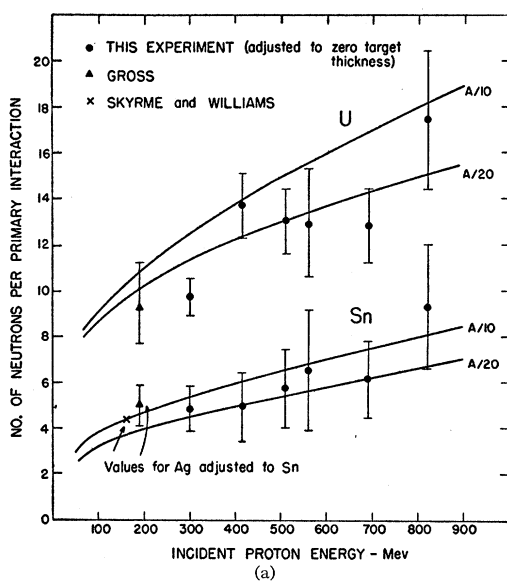
FIG. 9 (a, b, and c). Average number of neutrons per primary interaction as a function of incident proton energy. The curves are calculated from the Monte Carlo nucleon cascade calculations of Metropolis et al. and the Monte Carlo evaporation calculations of Dostrovsky et al. The labels $A/10$ and $A/20$ refer to the values of the level density parameter used in the evaporation calculations.

ferent atomic weights and values of incident proton energy. The excitation energy was then converted to mean neutron multiplicity using the Monte Carlo evaporation calculations of Dostrovsky, Rabinowitz, and Bivins,[4] interpolating and extrapolating where necessary to obtain values appropriate to the target elements used. In the case of uranium, the multiplicity so obtained was increased by 2 neutrons to account for fission. [In the interaction of high-energy nucleons with U^{238} nuclei, fission occurs in 75-80% of the cases[36] and takes place close to the end of the evaporation chain.[37] The residual average excitation energy of the fissioning nucleus is therefore not expected to exceed several tens of Mev. Measurements of fission neutron multiplicities resulting from incident fast neutrons up to 15 Mev show that the multiplicity may be expressed[38]

$$\nu(E_n) = \bar{\nu}_T + aE_n,$$

where $\bar{\nu}_T$ is the multiplicity in thermal fission, E_n is the neutron energy, and a is a constant for a particular nucleus. $\bar{\nu}_T$ lies in the range 2.1–2.5, and a in the range 0.12–0.14 for target nuclei between Th^{229} and U^{238}.[39]

[36] H. M. Steiner and J. A. Jungerman, Phys. Rev. 101, 807 (1956).
[37] I. Dostrovsky, Z. Fraenkel, and P. Rabinowitz, Proceedings of the Second United Nations International Conference on the Peaceful Uses of Atomic Energy, Geneva, 1958 (United Nations, Geneva, 1958), p/1615, Vol. 15, p. 301.
[38] I. I. Bondarenko, B. D. Kuzminov, L. S. Kutsayeva, L. I. Prokhorova, and G. N. Smirenkin, Proceedings of the Second United Nations International Conference on the Peaceful Uses of Atomic Energy, Geneva, 1958 (United Nations, Geneva, 1958), p/2187, Vol. 15, p. 353.
[39] R. B. Leachman, Proceedings of the Second United Nations International Conference on the Peaceful Uses of Atomic Energy, Geneva, 1958 (United Nations, Geneva, 1958), p/2467, Vol. 15, p. 229.
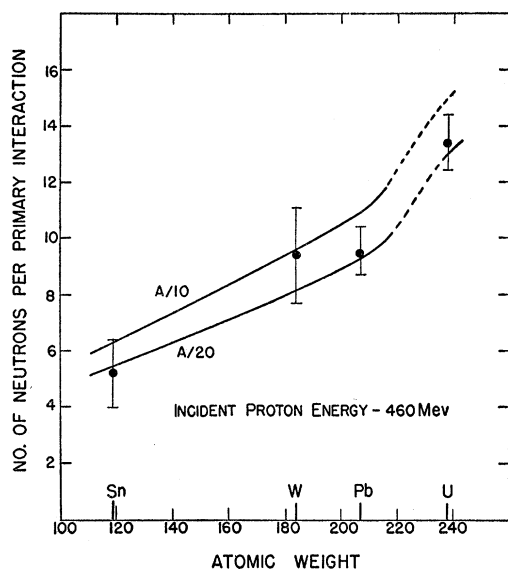
FIG. 10. Average number of neutrons per primary interaction due to 460-Mev incident protons as a function of atomic weight. The experimental points are the average values for the 415 Mev and 510-Mev proton groups. The theoretical curves are calculated as for Fig. 9.

TABLE XV. Calculated numbers of secondary neutrons per primary interaction.

Target: element and thickness (g cm^{-2})	Proton energy (Mev)					
	300	415	510	560	690	820
Sn (33)	1.0	1.4	1.5	1.7	1.9	2.2
W (34)	1.6	2.1	2.3	2.6	3.0	3.3
Pb (22)	1.2	1.6	1.8	2.0	2.3	2.8
Pb (44)	2.1	2.8	3.2	3.5	4.1	4.8
U (22)	1.7	2.3	2.6	2.9	3.4	4.0
U (44)	3.0	4.0	4.6	5.1	6.0	7.0

This implies a yield of 1 extra neutron for every 7–8-Mev excitation energy of the nucleus undergoing fission, and is roughly equal to that for the nonfission case. Thus, the neutron multiplicity is not seriously influenced by the point in the evaporation chain at which fission occurs, and we may simply add $(0.8 \times 2.5) = 2$ neutrons to account for fission.] The curves in Figs. 9(a), (b), (c), and 10 show the results of these calculations; the curves labelled $A/10$ and $A/20$ are those for the corresponding values of the level density parameter adopted in the evaporation calculations.

The experimental results presented in Sec. 5 for the 22 and 44 g cm^{-2} targets show clearly that at these thicknesses, secondary production of neutrons is considerable, therefore an estimate of this effect must be made before comparison with theory. Since the accuracy of the measurements is not good enough to permit a correction to be made from the experimental results we have calculated the size of the effect using the cascade proton results of the Metropolis Monte Carlo calculation.[3] For the purpose of this calculation the following assumptions were made:

(a) The energy and angular distributions of cascade neutrons are the same as those given by Metropolis *et al.* for cascade protons.

(b) The yield of low-energy neutrons produced by the cascade neutrons is the same as calculated for incident protons. Metropolis *et al.* show that the average excitation energy deposited by incident neutrons is very little different from that by protons of the same energy.

(c) Since nucleon-nucleus inelastic cross sections do not vary rapidly with energy in the 50–500-Mev range,

they were assumed to be constant for all cascade particle energies. The following effective interaction mean free paths were used; U—206 g cm^{-2}; Pb—195 g cm^{-2}; W—187 g cm^{-2}; Sn—180 g cm^{-2}.

(d) Tertiary interactions are neglected. Second generation cascade particles have on average only ~5% probability of interaction before leaving the 44 g cm^{-2} targets, and are greatly degraded in energy.

(e) The energy and angular distributions of cascade protons given for 460-Mev protons incident on uranium are applicable to all incident energies between 300 and 900 Mev, and target elements from Sn to U. To test this assumption, the average number of secondary neutrons per cascade particle was calculated for the 44 g cm^{-2} target using the energy and angular distributions given by Metropolis *et al.* for (i) 1840-Mev protons on U, (ii) 460-Mev protons on Al. The result for case (i) was 12% higher and that for case (ii) 15% lower than that using the distributions for 460 Mev on U. The insensitivity of the energy and angular distributions to incident energy and atomic weight over such a wide range implies that the secondary neutron multiplication depends principally on the cascade particle multiplicity, and justifies the assumption made above.

The numbers of secondary neutrons per primary interaction calculated under the given assumptions for the various targets and energies are listed in Table XIV.

The estimates of neutron multiplication run from 15% to 45% of the calculated primary interaction multiplicities shown in the curves of Figs. 9(a), (b), and (c).

In the graphical presentation of our results, we have chosen to adjust the multiplicities measured for our targets to zero thickness by subtracting the estimated numbers of secondary neutrons in Table XV from the experimental values in Table XIII. These adjusted values are shown plotted in Figs. 9(a), (b), and (c). The points for uranium and lead are the error-weighted means of the values obtained for the 22 and 44 g cm^{-2} targets. The errors are deduced from those given in Table XIII. No allowance for a possible error in the estimates of multiplication has been made.

To extend the experimental energy range, we have also plotted the results of other experiments at energies below 200 Mev by Gross,[6] and Skyrme and Williams.[5]

These data have been adjusted for small differences in atomic weight where the target elements differed from those used in this experiment. The points representing the results of this experiment are, within errors, consistent with those at lower energies.

In Fig. 10 we have plotted the number of neutrons per primary interaction against atomic weight at an incident proton energy of 460 Mev. The experimental points are the average of values for 415 and 510 Mev. These energy groups were chosen as the most reliable, being relatively free from any uncertainty of the muon contamination correction, and in an energy range where the uncertainties in the multiplication estimate are least.

The experimental points and the theoretical curves of Figs. 9 and 10 are, within errors, in agreement; no inadequacy of the theory, as presently developed, is revealed by the experimental results.

ACKNOWLEDGMENTS

[40] W. B. Lewis, Atomic Energy of Canada Limited Report A.E.C.L.-DR-24 (1952).